Z. Angew. Math. Phys. 66 (2015), 2703–2718

0044-2275/15/052703-16
published online April 22, 2015
DOI 10.1007/s00033-015-0527-9

Zeitschrift für angewandte Mathematik und Physik ZAMP

The effect of Thompson and Troian's nonlinear slip condition on Couette flows between concentric rotating cylinders

H. Power, J. Soavi, P. Kantachuvesiri and C. Nieto

Abstract. In this work, a detailed study of the effect of the Thompson and Troian's nonlinear slip condition on the flow behaviour of a Newtonian incompressible fluid between two concentric rotating cylinders (Couette flow) is considered. In Thompson and Troian's nonlinear condition, the slip length on the Navier slip condition is considered to be a function of the tangential shear rate at the solid surface instead of being a constant. The resulting formulation presents an apparent singularity on the slip length when a critical shear rate is approached. By considering this type of nonlinear slip condition, it is possible to predict complex characteristics of the flow field not previously reported in the literature, and to show the effect of nonlinear slip on the inverted velocity profiles previously observed in the linear slip case. Particular attention is given to the behaviour of the flow field near the critical shear rate. In such a limit, it is found that the flow field tends to slip flow with a finite slip length. Consequently, previous critique on the singular behaviour of Thompson and Troian's nonlinear model is not valid in the present case.

Mathematics Subject Classification. 76A99 · 76U05 · 35G50 · 65H10.

Keywords. Nonlinear Navier slip boundary condition, Analytical study, Microfluidics.

1. Introduction

Fluid flows in micro- and nanofluidic devices are characterized by the confinement of the fluid environment to micro- and nanoscales. The reduction in scale implies that surface effects start to dominate over volume-related phenomena, requiring accurate details of the flow–surface interaction. When fluid devices are scaled down to those sizes, the surface-to-volume ratio increases dramatically so that surface-related phenomena become increasingly dominant. At this scale, several new features emerge, such as the slip flow regime that occurs due to an insufficient number of molecules across the flow thickness, see [1]. Under this condition, it becomes important to understand the various types of interactions that arise between the fluid constituents and the solid surfaces that contain it, for more details see the review article by Neto et al [2].

The characteristic length scale of fluid flows is determined by the Knudsen number, $K_n = \lambda/L$, where λ as the mean free path (collision distance between molecules; for air at atmospheric conditions $\lambda = 68\,\text{nm}$) and L as the characteristic fluid thickness. For values of $10^{-3} < K_n < 10^{-1}$,i.e., at the micro- and nanoscales, the flow is usually considered as a continuum with a slip boundary condition. There are large amounts of experimental and theoretical evidence reported in the literature on the occurrence of slip velocity at the micro- and nanoscales (see [3] and [4] for laboratory observation of slip conditions using advanced experimental techniques as well as [5] and [6] for molecular dynamics (MD) simulations, among others). The existence of slip velocity was first predicted by Navier [7] (see also [8]). Navier's slip model proposed a linear relationship between the wall tangential fluid shear rate and the fluid-wall velocity difference, with the slip length as the proportionality constant. This type of slip model has been successfully used in reproducing the characteristics of many types of slip flows, see among others [9–11].

Variation in slip length arises from the fact that, during a collision with a solid surface, a fluid molecule will transfer some of its tangential momentum to the solid. The collision frequency is not high enough to ensure thermodynamic equilibrium, and a certain degree of slip tangential velocity must be allowed.

For gas–solid interaction, the slip length is characterized by the tangential momentum accommodation coefficient, σ, where $\sigma = 1$ represents diffuse reflection (gas molecule tangential momentum not conserved, minimum slip length) and $\sigma = 0$ represents specular reflection (gas molecule tangential momentum conserved, infinite or perfect slip length). The relationship between the slip length and accommodation coefficient is (for more details see [12] and [13])

$$L_s = \lambda \left(\frac{2.01}{\sigma} - 0.73 - 0.16\sigma \right) \tag{1.1}$$

Note that even diffuse reflectance, $\sigma = 1$, should produce a slip length roughly equal to the mean free path, i.e., a slip length of the order of $O(10^{-1})$ to $O(10^{-3})$ of the flow thickness, while in the case of $\sigma < 1$, the slip length can be of the order of magnitude or greater than the flow thickness.

The slip condition for gas flow at the solid–gas interface can be significantly modified by the adsorption of the thin film into the solid. [14] reported an increase in the slip length of a monolayer of octadecyltrichlorosilane from 290 to 590 nm by increasing the temperature from 18 to 40 °C, which is associated with a possible adsorption of the gas into the octadecyltrichlorosilane layer.

For the case of liquids, the above estimation of the slip length is not as well defined. When the solid surface is hydrophobic, apparent slip velocity has been observed with slip length of the order of 1 μm (10^3 nm) and even of the order of 50 μm in the case of super hydrophobic surfaces, see [15,16]. On the other hand, when the surface is hydrophilic, the no-slip boundary condition is usually employed in the analysis of liquid flows at micro- and nanoscale. However, wall slip velocities on hydrophilic surfaces have been experimentally observed under specific chemical and electrochemical conditions between the liquid and solid. A possible explanation of the occurrence of liquid slip on hydrophilic surfaces is the effect of these additional reactions on the wettability of the liquid. Under these conditions, there is the possibility of adsorption into the solid surface, which can modify the surface properties and lead to the emergence of a partial or total slip condition, for more details see [17] and [18] among others. More recently, using molecular dynamics (MD) simulations, Hoa et al. [19] demonstrated that both slip and no-slip conditions can be observed on liquid water flowing on hydrophilic surfaces. The appearance of the slip condition appears to be a consequence of the distribution of water molecules within the contact layer at equilibrium, coupled with the strength of water–surface interactions. Hydrodynamic liquid slip occurs when preferential adsorption sites exist that are sufficiently close to each other that water can migrate from one site to the next one without requiring hopping events.

Although the use of the linear Navier slip condition has been successfully implemented in analytical and numerical studies of different types of flows at nano- and microscale, there are several well-known instances where this condition leads to singular or unrealistic flow behaviour, such as the spreading of liquids over a dry solid surface, corner flows and the extrusion of polymer melts from a capillary (for more details see [6] and [20]). In general, linear slip conditions fail to reproduce the flow behaviour in localized regions of high surface shear.

Experimental studies using atomic force microscope (AFM) and surface force apparatus (SFA), show that constant slip length (linear slip boundary condition) do not correctly describe the measured slip velocity at a high shear rate (for more details see [21]). In [4], it was observed that the slip length is roughly constant at small shear rate, but increases dramatically with the shear rate at large slip. Direct measurements of hydrodynamic draining forces in Newtonian liquids, [4], show a variable slip flow at the solid–fluid interface which is a function of the liquid viscosity and the shear rate.

From the results of MD simulations in [5], a nonlinear slip boundary condition is proposed (from now on we refer to it as Thompson and Troian's nonlinear slip model) that accounts for the nonlinear behaviour of the slip length, where the slip length also depends on the tangential shear rate at the solid

surface instead of being a constant. In Thompson and Troian's nonlinear slip condition, the slip length can account for any of the following three cases: constant slip length (linear model), nonlinear slip length (nonlinear model) and the no-slip condition, see [21]. However, Thompson and Troian's model presents an apparent singularity in the slip length when a critical shear rate is approached, corresponding to a divergent condition. The analysis of the flow field and its behaviour when the shear rate approaches the critical value is one of the main objectives of the present work.

As commented in [10] (chapter 4, section 4.6), the nonlinear behaviour close to a critical shear rate in Thompson and Troian's model suggests that the boundary condition can significantly affect the flow behaviour at macroscopic distances from the wall, which was experimentally confirmed in [22]. The rapid change in the slip length suggests that for flows in the vicinity of the critical shear rate, small changes in surface properties can lead to large fluctuations in the apparent boundary condition. According to [10], Thompson and Troian's nonlinear and divergent slip model may provide a mechanism for relieving the stress singularity in spreading contact lines and corner flows, given variable degrees of slip as the flow approaches regions of higher rate of strain.

More recently, [16] proposed a nonlinear slip model (that from now on we refer to as Yang's slip model) based on concepts from the theory of thermal activation processes, where the slip velocity is proportional to the hyperbolic sine of the shear stress on the solid surface. The corresponding slip boundary condition reduces to Navier slip boundary condition for small shear stresses. Besides, Yang's slip model is qualitatively consistent with the shear rate dependence of the slip length in Thompson and Troian's model, but does not present an apparent singularity at a critical shear rate. There is also a critical shear stress in Yang's model, but instead of defining a divergent slip length, as in Thompson and Troian's model, it determines the onset of the slip flow, as originally proposed in [25] where the slip model has a critical shear stress at which no-slip begins, followed by slip at a constant slip length. Unfortunately, it appears that no experimental and/or MD simulations have been reported in the literature validating Yang's slip model.

In comparison with linear slip flows, research on nonlinear slip flows is more limited, with relatively few works reported in the literature. In [23] and [21], numerical solutions of nonlinear slip flows using Thompson and Troian's model are reported, where lid-driven polar cavity flow and thin film flow of a fluid between two spheres are considered. On the other hand, in [24], analytical solutions are obtained for slip flows through infinite circular pipes and two dimensional channels with a slip condition given by Thompson and Troian's nonlinear model.

In this work, a detailed analytical study of the effect of Thompson and Troian's nonlinear slip condition on the flow behaviour of a Newtonian fluid between two concentric rotating cylinders (Couette flow) is considered. Particular attention is given to the behaviour of the resulting flow field in the vicinity of the critical shear rate. Studies of rotating Couette flow with linear slip fluid velocity at the cylinder walls have demonstrated that under certain conditions, the flow field can exhibit no intuitive behaviour, as in the case of a stationary outer cylinder and a rotating inner cylinder where the velocity profile can become inverted, with the velocity increasing from the inner rotating wall to the outer stationary wall (for more details see [1] and [26]). More recently, [27] study slip flows in concentric rotating cylinders using a slip model defined in terms of the Langmuir adsorption isotherm for the gas–solid surface molecular interaction, instead of the Navier's accommodation coefficient. In their work, they showed that despite the conceptual difference in the two slip models (Navier and Langmuir), both are in qualitative agreement with Monte Carlo simulation data in capturing the general features of the flow field.

2. Nonlinear slip condition

At the micro- and nanoscale, the flow of a Newtonian viscous fluid with viscosity μ and density ρ can be modelled by the Navier–Stokes system of equations with an appropriate slip condition. The most

common used slip conditions in the literature are based on Navier slip boundary condition, [7], that defines a relative tangential fluid velocity, u_t^f, with respect to the tangential wall velocity, U_t^w, linearly proportional to the tangential projection of the local shear rate, $\dot{\gamma}_t$, as given in dimensionless form by Eq. (2.1). The proportionality constant is called the slip length, L_s, and represents the hypothetical outward distance at the wall needed to satisfy the no-slip flow condition (for more details see [28] and [29]).

$$u_t^f - U_t^w = L_s \dot{\gamma}_t, \tag{2.1}$$

with

$$\dot{\gamma}_t = \left(\frac{\partial u_i}{\partial x_j} + \frac{\partial u_j}{\partial x_i} \right) n_j s_i = \left(\frac{\partial u_t}{\partial n} + \frac{\partial u_n}{\partial s} \right), \tag{2.2}$$

where n_i and s_i are the i components of the normal and tangential vectors at the boundary surface.

As mentioned previously, there is substantial theoretical and experimental evidence that the slip length has a constant value at low tangential shear rate, but increases dramatically as the shear rate reaches a critical value $\dot{\gamma}_c$. Above this critical value, there is no additional momentum transfer between the wall and the fluid molecules [20]. Thompson and Troian [5] proposed a nonlinear boundary condition with slip length also depending on the tangential shear rate at the solid surface via the following relation:

$$L_s = \frac{b_o}{\sqrt{(1 - \beta \dot{\gamma}_t)^n}}, \tag{2.3}$$

where β is a parameter representing the inverse of critical shear rate $\dot{\gamma}_c$, i.e., $\beta = 1/\dot{\gamma}_c$, with the critical shear rate set by the corrugation of the potential surface which signals the point at which the solid can no longer impart momentum to the liquid. In the above expression, b_o is a constant parameter corresponding to the value of the slip length at low shear rate and n is an index that depends on the cohesive property at the interface. Thompson and Troian's nonlinear slip model is obtained by substituting the nonlinear slip length given by expression (2.3) into the Navier slip boundary condition, Eq. (2.1). As can be observed, an apparent singularity in the boundary condition occurs when the shear rate approaches the critical value β^{-1}. However, this apparent singularity cannot be analysed without obtaining the complete solution of the problem for a given set of the parameters b_o, β and n, since the shear rate in (2.3) is part of the solution of the problem.

In Thompson and Troian's model, the constant slip length and the no-slip condition are found as limiting cases of expression (2.3). The first one refers to the condition when $\beta \to 0$ ($\dot{\gamma}_c \to \infty$), for finite values of b_o, corresponding to $L_s \to b_o$ (constant slip length). On the other hand, the limiting case when $n \to \infty$, for finite values of $\dot{\gamma}_c$ and b_o, corresponding to $L_s \to 0$, results in the classical no-slip condition.

To complete the boundary conditions at the solid surfaces, it is necessary to include the non-flux condition across the boundaries, i.e.,

$$u_i(x)\, n_i(x) = U_n^w(x), \tag{2.4}$$

In the present work, a parametric study for different values of β and b_o is considered to analyse their effect on the slip flow behaviour. However, for simplicity, the index n will be kept constant and equal to one. The value of $n = 1$ has been successfully used before to predict several simple and complex slip flow problems, and their solutions compare well with corresponding MD simulations (see [5]).

3. Internal rotating cylinder

Let us consider the isothermal steady-state flow motion of a Newtonian fluid between two concentric cylinders with the inner cylinder rotating at constant angular velocity, while the outer cylinder is kept stationary. Our formulation of the problem is given in dimensionless form in terms of the characteristic length scale r_e (the external radius), with $(r_i/r_e) = d < 1$ as the ratio between the internal and external radius, and the characteristics time $1/\omega$, pressure $\mu\omega$, velocity ωr_l and shear rate $\omega r_l/r_e$, with $r_l = r_i$ or

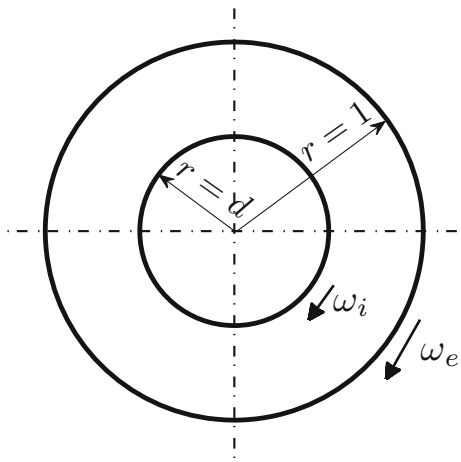

FIG. 1. Schematic representation of the problem geometry

$r_l = r_e$, accordingly if the internal or external cylinder is in rotation. Here, ω is the angular velocity of the rotating cylinder and the Reynolds number is defined as $Re = \rho\omega r_l r_e/\mu$.

In the case of an internal rotating cylinder, the dimensionless wall velocities at the rotor and stator are: $U_i^w(x) = 1$ at $r = d$ and $U_e^w(x) = 0$ at $r = 1$, with $r = d$ and $r = 1$ as the internal and external dimensionless radius, respectively, see Fig. 1.

Given the azimuthal symmetrical condition of the problem, it follows that at steady state, the dimensionless Navier–Stokes system of equations can be written exactly in cylindrical polar coordinates as:

$$\begin{aligned} -Re\left(\frac{{u_\theta}^2}{r}\right) &= -\frac{dp}{dr}, \\ \frac{d}{dr}\left[\frac{1}{r}\frac{d}{dr}(ru_\theta)\right] &= 0, \end{aligned} \tag{3.1}$$

where u_θ and p are the dimensionless azimuthal velocity and pressure fields, respectively. Due to the simple geometrical configuration considered and under steady-state isothermal conditions, the equation of conservation of mass is identically satisfied for both compressible and incompressible fluids, exactly reducing the Navier–Stokes system of equations to (3.1), for both types of fluids.

Similarly, the nonlinear slip boundary condition at the inner and outer cylinders, defined by (2.1) to (2.3), are expressed as:

$$u_{\theta|r=d} = 1 + b_o\left[1 - \beta\left|r\frac{d}{dr}\left(\frac{u_\theta}{r}\right)\right|_{r=d}\right]^{-1/2}\left(r\frac{d}{dr}\left(\frac{u_\theta}{r}\right)\right)_{r=d}, \tag{3.2a}$$

$$u_{\theta r=1} = -b_o\left[1 - \beta\left|r\frac{d}{dr}\left(\frac{u_\theta}{r}\right)\right|_{r=1}\right]^{-1/2}\left(r\frac{d}{dr}\left(\frac{u_\theta}{r}\right)\right)_{r=1}, \tag{3.2b}$$

The solution of Eq. (3.1) can be written as:

$$u_\theta = Ar - \frac{B}{r}, \tag{3.3a}$$

$$\frac{p}{Re} = \frac{A^2r^2}{2} - \frac{B^2}{2r^2} - 2AB\ ln\,(r)\,, \tag{3.3b}$$

with the corresponding tangential component of the surface traction given by

$$\dot{\gamma}_t = r\frac{d}{dr}\left(\frac{u_\theta}{r}\right) = \frac{2B}{r^2}, \tag{3.3c}$$

In the above expressions, the value of the constants A and B are obtained by substituting (3.3a) into (3.2a), (3.2b), leading to the following set of nonlinear algebraic system of equations:

$$Ad - \frac{B}{d} = 1 + b_o\left(1 - \frac{2\beta}{d^2}\|B\|\right)^{-\frac{1}{2}}\left(\frac{2B}{d^2}\right), \tag{3.4a}$$

$$A - B = -b_o\left(1 - 2\beta\|B\|\right)^{-\frac{1}{2}}(2B) \tag{3.4b}$$

Combining the above two equations into one, we obtain

$$\left(1 - \frac{1}{d^2}\right)B = \frac{1}{d} + \frac{b_o}{d}\left(1 - \frac{2\beta}{d^2}\|B\|\right)^{-\frac{1}{2}}\left(\frac{2B}{d^2}\right) + b_o\left(1 - 2\beta\|B\|\right)^{-\frac{1}{2}}(2B), \tag{3.5}$$

or

$$\left[\left(1 - d^2\right) + 2b_o\left(\frac{1}{d}\chi_i + d^2\chi_e\right)\right] = -\frac{d}{B} \tag{3.6}$$

with $\chi_e = \left(1 - 2\beta\|B\|\right)^{-\frac{1}{2}}$ and $\chi_i = \left(1 - \frac{2\beta}{d^2}\|B\|\right)^{-\frac{1}{2}}$.

An analytical solution of the nonlinear algebraic Eq. (3.6) cannot be easily found. However, a numerical approach or a graphical representation of the equation can be used to find the value of B for a given set of parameters. In this work, both approaches are used to find the value of the constant B, i.e., a Newton iterative scheme and a graphical representation. In [24], analytical closed-form solutions are found for Thompson and Troian's nonlinear slip flow in a circular pipe and a parallel channel having uniform cross section; however, in the case of annular flows between two infinite coaxial circular pipes, a system of two nonlinear algebraic equations of the type of (3.4a), (3.4b) are obtained, the solution of which is found by using a graphical representation approach.

After obtaining the value of B, the value of A is found from (3.4b), as

$$A = B - b_o\left(1 - 2\beta\|B\|\right)^{-\frac{1}{2}}(2B), \tag{3.7}$$

completing the solution of the problem. By substituting the obtained value of A in terms of B into the expressions for the velocity and pressure fields, Eqs. (3.3a), (3.3b), it is possible to express these field variables only in terms of the constant B, as:

$$u_\theta = B\left[\left(1 - 2b_o\chi_e\right)r - \frac{1}{r}\right], \tag{3.8a}$$

$$\frac{p}{Re} = B^2\left[\left(1 - 2b_o\chi_e\right)^2\frac{r^2}{2} - 2\left(1 - 2b_o\chi_e\right)ln\ r - \frac{1}{2r^2}\right], \tag{3.8b}$$

In this way, the solution of the problem is determined solely by the constant B as a function of the other parameters of the problem (d, β and b_o).

To find a graphical representation of the solution of (3.6), the following two curves are defined:

$$Y_1 = -\frac{d}{B}, \tag{3.9a}$$

and

$$Y_2 = \left[\left(1 - d^2\right) + 2b_o\left(\frac{1}{d}\chi_i\left(\beta, \|B\|\right) + d^2\chi_e\left(\beta, \|B\|\right)\right)\right] \tag{3.9b}$$

The value of B for a given set of the parameters (d, b_o, β) is found at the point of interception between these two curves, i.e., at the point where $Y_1 = Y_2$. By direct inspection of (3.6), it is easy to see that the value of B corresponding to the no-slip condition, i.e., $b_o = 0$, is given by $B = -d/(1 - d^2)$, while the one corresponding to the linear slip case, i.e., $\beta = 0$, for which $\chi_i = \chi_e \equiv 1$, is given by $B = -d/\left(\left(1 - d^2\right) + 2b_o\left(d^2 + 1/d\right)\right)$.

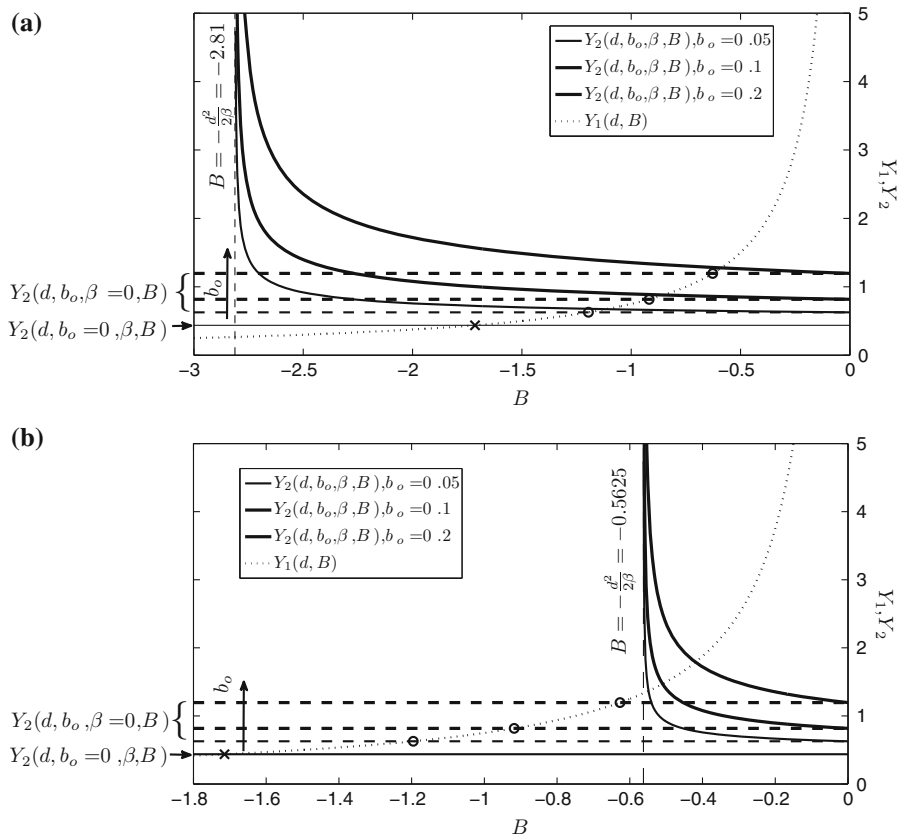

FIG. 2. Graphical solution of the nonlinear system of Eqs. (3.9a), (3.9b) for two different values of β: **a** $\beta = 0.1$ and **b** $\beta = 0.5$, with three values of b_o

In our analysis of the nonlinear slip case, we use $d = 0.75$, i.e., a flow gap of 0.25, and different values of the parameters (b_o, β). As mentioned in the introduction, the value of the linear slip length coefficient b_o can range from the order of the surface roughness to the order of the fluid gap or several times larger, $b_o \geq O(1)$, according to the characteristic of the fluid (gas or liquid), and the solid surface, while the value of β is determined by the corrugation of the potential surface. Figure 2a, b shows plots of the curves Y_1 and Y_2 for three different values of b_o: $0.05, 0.1$ and 0.2, and two values of β: 0.1 (Fig. 2a) and 0.5 (Fig. 2b). In the figures, the direction of the arrow indicates increasing magnitude of the value of b_o.

In [21], nonlinear slip flows were analysed for values of $\dot{\gamma}_c^* = 3.8$ and $143\ \mathrm{s}^{-1}$, where $*$ indicates a dimension quantity. For the values of β considered in Fig. 2a, b, these critical shear rates correspond to angular velocities ω of 0.507 and 2.533 radians per second, when $\dot{\gamma}_c^* = 3.8\ \mathrm{s}^{-1}$, and 19.066 and 95.333 radians per second, when $\dot{\gamma}_c^* = 143\ \mathrm{s}^{-1}$, consistent with realistic magnitudes of rotation of nanobearings. For completeness of the present study, larger values of b_o and β than those reported in Fig. 2a, b are also considered, with b_o up to a value of 5 and β up to 2, see in Fig. 3.

In Fig. 2a, b, the interception between the three different curves $Y_2\,(d, b_o, \beta, B)$, for different values of b_o, with the single curve $Y_1\,(d, B)$ corresponds to the solutions of B in the nonlinear slip cases. The interception between the three horizontal dashed lines $Y_2\,(d, b_o, \beta = 0, B)$, with the curve Y_1, i.e., the three circular points in the figures, corresponds to the solutions of B in the linear slip cases. Finally, the interception between the horizontal continuous line $Y_2(d, b_o = 0, \beta, B)$ with the curve Y_1, i.e., the point indicated by the $\times$ symbol in the figures, corresponds to the solution of B in the no-slip case.

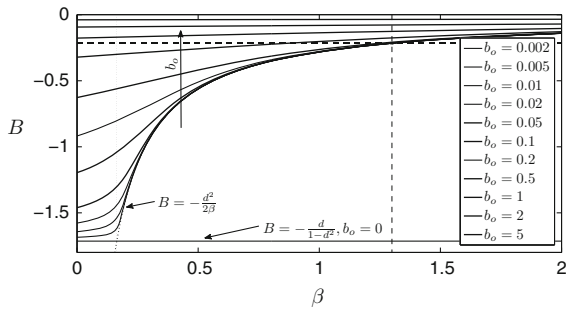

FIG. 3. Newton iterative solution of the nonlinear Eq. (3.6) for different values of β and b_o

It is also possible to observe in Fig. 2a, b an asymptote to the curves $Y_2\left(d, b_o, \beta, B\right)$ in the limit when χ_i tends to infinity, i.e., $\chi_i \to \infty$ as $B \to -d^2/2\beta$, corresponding to the apparent singularity in Thompson and Troian's slip length model. This asymptote defines the range of possible values of B in the nonlinear slip case. It is interesting to observe that in the case when $\beta = 0.1$, all values of B for the no-slip, linear and nonlinear slip cases are found inside the range $-d^2/2\beta < B < 0$. However, when $\beta = 0.5$, only the nonlinear slip cases are found inside this range, having values of $B < -d^2/2\beta$ for the linear slip and no-slip cases. Later in this section, we will further analyse the observed difference in the values of B for the different slip conditions (no-slip, linear and nonlinear slip) when different values of β are considered.

An interesting feature of this graphical representation is the possibility to observe simultaneously from the figure the solutions corresponding to the three different slip conditions (no-slip and linear slip and nonlinear slip), which are not always easy to observe from a closed-form analytical expression.

Figure 3 shows values of B obtained for different values of β and b_o using the iterative Newton method, which can also be exactly reproduced using the graphical approach. As before, the arrow in the figure indicates an increasing magnitude of b_o. In the figure, there are three features worth noting:

1. The horizontal line at the bottom of the figure, corresponding to the value of B in the case of no-slip boundary condition, i.e., $B = -d/\left(1 - d^2\right)$, which is equal to $B = -1.7143$ for $d = 0.75$.
2. The values of the intersection between the different curves for different values of b_o with the vertical axis of the coordinates system, corresponding to the values of B in the cases of linear slip, i.e., $\beta = 0$.
3. The curve $B = -d^2/2\beta$ corresponding to the asymptotic value of B defined by the condition when $\chi_i \to \infty$.

As shown in Fig. 3, in the nonlinear case the values of B are confined to the domain space between the value $B = 0$, the curve $B = -d^2/2\beta$ and the horizontal line $B = -d/\left(1 - d^2\right)$, with values of B on the axis $\beta = 0$ corresponding to the linear case. In other words, no solution is found in the parameter space limited from below by the horizontal line $B = -d/\left(1 - d^2\right)$ and from above the curve $B = -d^2/2\beta$.

Also in Fig. 3, it is possible to observe the value of $\beta = d\left(1 - d^2\right)/2$ at which the asymptotic curve $B = -d^2/2\beta$ attains the value of $B = -d/\left(1 - d^2\right)$ corresponding to the no-slip condition. This value of β is obtained at the point where the curve $B = -d^2/2\beta$ intersect the horizontal line at the bottom of the figure. When $\beta \leq d\left(1 - d^2\right)/2$ ($\beta \leq 0.1641$ for $d = 0.75$), the values of B in all the cases considered, i.e., no-slip, linear and nonlinear slip, are found inside the range $-d/\left(1 - d^2\right) \leq B \leq 0$, as was the case in Fig. 2a for $\beta = 0.1$. On the other hand, for values of $\beta > d\left(1 - d^2\right)/2$, the no-slip and linear slip cases are found within the range $-d/\left(1 - d^2\right) \leq B \leq 0$, while the non linear case is found in the range $-d^2/2\beta \leq B \leq 0$, as was the case in Fig. 2b for $\beta = 0.5$.

Figure 4 shows the obtained velocity profiles for a value of $b_o = 0.1$ and values of $\beta = 0$ (linear case), and $\beta = 0.05, 0.1, 0.2, 0.4, 0.6$ and 0.8 (nonlinear cases) with corresponding values of $B = -0.9184$ (linear case), and $B = -0.8866, -0.8519, -0.7730, -0.5927, -0.4411, -0.3515$ (nonlinear case) according to the results reported in Fig. 3. The above values of B for the nonlinear cases are all smaller than

TABLE 1. *Slip length values at the stator and rotor for $b_o = 0.1$ and different values of β*

β	0	0.05	0.1	0.2	0.4	0.6	0.8
L_s							
$r = 1$ (stator)	0.1	0.1048	0.1098	0.1203	0.1379	0.1458	0.1512
$r = 0.75$ (rotor)	0.1	0.1090	0.1198	0.1490	0.2523	0.4117	7.50

their corresponding asymptotic limit $B = -d^2/2\beta$, with value $B = -0.3515$ for $\beta = 0.8$ very close to its asymptotic value of $B = -0.3515625$.

Table 1 shows the obtained values of the slip length, L_s at the stator and rotor for each of the velocity profiles in Fig. 4 with the corresponding value at the rotor always larger than the one at the stator. In the table, the values of the slip length at the stator and rotor for the case of $\beta = 0.4$ are $L_s = 0.1379$ and $L_s = 0.2523$, respectively. Figure 5 presents a comparison between the velocity profile for $\beta = 0.4$ (nonlinear case) in Fig. 4 with the corresponding linear cases ($\beta = 0$) for values of slip lengths $L_s = 0.1379$ and $L_s = 0.2523$, showing that the effect of the nonlinear slip condition is not only an increase in magnitude of the slip length but a change in the shape of the velocity profile.

As can be observed from Fig. 3, the asymptotic limit of $B \to -d^2/2\beta$, which corresponds to a flow field with shear rate at the rotor equal to its critical value, i.e., $\dot{\gamma}_t = -1/\beta$, is only attained when $\beta > d\left(1 - d^2\right)/2$ in the limit as $b_o \to 0$, with a corresponding shear rate at the stator of $\dot{\gamma}_t = -d^2/\beta$. In this limit, the obtained velocity profile is given by:

$$u_\theta = -\frac{d^2}{2\beta}\left(r - \frac{1}{r}\right), \tag{3.10}$$

with boundary velocities $u_\theta(r = 1) = u_t^s = 0$ and $u_\theta(r = d) = u_t^r = -d^2(d - 1/d)/2\beta$, resulting in a no-slip condition at the stator and a slip velocity at the rotor with slip length $L_s = \beta - d\left(1 - d^2\right)/2 > 0$. Consequently in the present case, the apparent singular slip length in Thompson and Troian's nonlinear model results in a regular flow field attained only in the limit as $b_o \to 0$.

As previously mentioned, a major aspect of the analytical solution of the linear slip case ($\beta = 0$, i.e., $L_s = b_o$), which is counter intuitive, is the possibility that for a given set of parameters (flow gap and slip length) the fluid in contact with the stationary housing (stator) can move faster than the one in contact with the moving rotor. This counter intuitive behaviour is known in the literature as an inverted velocity profiles (see [1] and [26]). The condition when the inverted velocity profile starts to occur is found at values of b_o for which the velocity of the fluid in contact with the stationary housing is equal to the velocity of the fluid in contact with the moving rotor. This flow condition is achieved in the linear slip

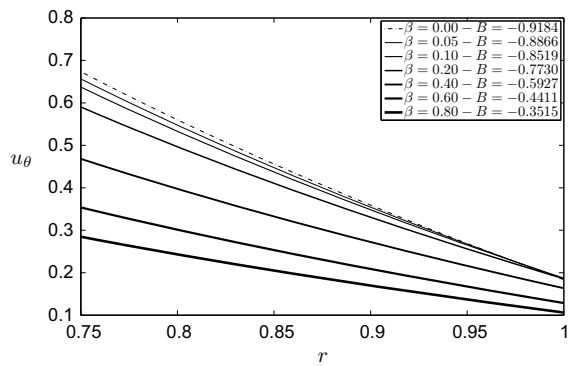

FIG. 4. Velocity profiles for linear and nonlinear slip conditions

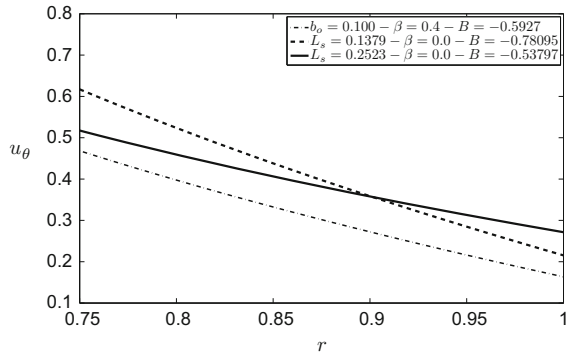

FIG. 5. Velocity profiles for linear and nonlinear slip conditions for the case when $\beta = 0.4$

case ($\beta = 0$ and $B = -d/\left(\left(1-d^2\right) + 2b_o\left(d^2 + 1/d\right)\right)$) at $b_o = (1+d)/2d$ (for more details see [30]), i.e., $b_o = 1.1667$ for $d = 0.75$. Also in the linear slip case, the velocity profiles for different values of b_o intersect the corresponding profile for the no-slip case at a single point, which is located at distance $r = \left(\left(d^3+1\right)/(d+1)\right)^{1/2}$ (see [30] and [31]), i.e., $r = 0.9014$ for $d = 0.75$.

In the present case of nonlinear slip condition, it is also possible to show the existence of an inverted velocity profile. By looking at the value b_o when the velocity at the moving rotor is equal to the velocity at the stationary stator, i.e., from (3.8a) when $((1-2b_o\chi_e) - 1) = ((1-2b_o\chi_e)\ d - 1/d)$, it follows that this condition is found when $b_o = (1+d)/(2\ d\chi_e)$, with $0 < \chi_e \leq 1$. Consequently, inverted velocity profiles occur for values of $b_o > (1+d)/(2d\chi_e)$. For the values of β considered in Fig. 2, i.e., $\beta = 0.1$ and 0.5 with $d = 0.75$, it follows from this estimation that inverted velocity profiles occur for values of b_o greater than 1.15 and 1.08, respectively, both of them smaller than the corresponding value for the linear slip case. To clearly show the value of b_o at which the inverted velocity profile appears, we plot in Fig. 6a, b the slip velocity at the rotor and stator as a function of b_o for the two β cases considered in Fig. 2. At the point when the two curves in the figures intersect, the velocity at the moving rotor is equal to the velocity at the stationary stator. As can be observed, those intersection points exactly coincide with the obtained analytical values of b_o.

Also in Fig. 6a, b, a new feature appears in the behaviour of the nonlinear slip velocity. In both cases, $\beta = 0.1$ and 0.5, the slip velocity at the stator (u_t^s in the figures) is an increasing monotonic function of b_o, while for the case of $\beta = 0.1$, in Fig. 6a, the slip velocity at the rotor (u_t^r in the figures) is a decreasing monotonic function of b_o. However, in Fig. 6b, when $\beta = 0.5$, the slip velocity at the rotor is not a monotonic function, having a local maximum near $b_o = 0$. In this last case, the rotor slip velocity has a jump condition at $b_o = 0$ with a value of $u_t^r = 1$ at $b_o = 0$, according to the boundary condition (3.2a), but with a limit value smaller than one as $b_o \to 0$, i.e., a discontinuous limit. This is probably the most surprising behaviour of Thompson and Troian's nonlinear slip model happening at the limiting of the critical shear rate.

To see clearly the behaviour of the slip rotor velocity as b_o tends to zero, the results in Fig. 3 are further analysed, where two distinct regions of B values are identified, corresponding to values of $\beta \gtrless d\left(1-d^2\right)/2$, i.e., $\beta \gtrless 0.1641$ for $d = 0.75$. In the limit when $b_o \to 0$ for $\beta \leq d\left(1-d^2\right)/2$, i.e., in the region to the left of the vertical dashed line in Fig. 3, the value of B tends monotonically to the no-slip solution $B = -d/\left(1-d^2\right)$, and consequently also in this limit $u_t^r \to 1$ monotonically, as is the case in Fig. 6a for $\beta = 0.1 < 0.1641$. On the other hand, when $b_o \to 0$ for $\beta > d\left(1-d^2\right)/2$, i.e., the region to the right of the vertical dash line in Fig. 3, the value of B tends to the asymptotic value $B = -d^2/2\beta$, and consequently the slip rotor velocity tends to:

$$\lim_{b_o \to 0}\left(u_t^r\right) \to \frac{-d^2}{2\beta}\left(d - \frac{1}{d}\right), \tag{3.11}$$

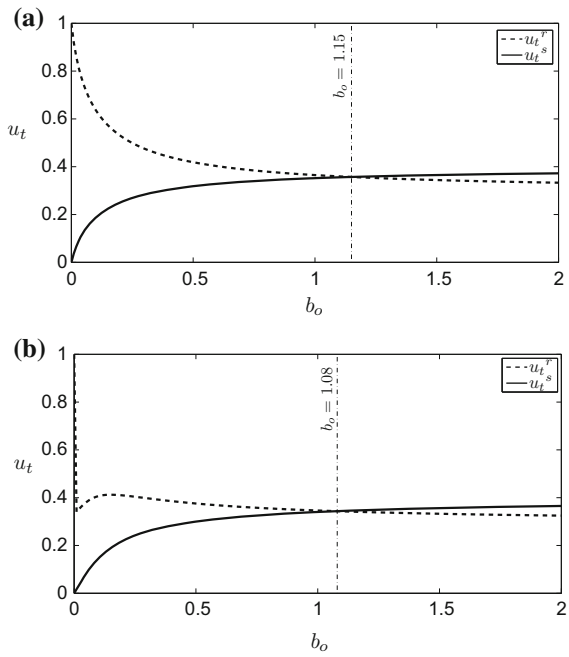

FIG. 6. Slip velocity at the rotor and stator as a function b_o, **a** $\beta = 0.1$ and **b** $\beta = 0.5$

which is different from the value of $u_t^r = 1$ at $b_o = 0$, having a discontinuous limit as $b_o \to 0$. From (3.11) with $\beta = 0.5 > 0.1641$ and $d = 0.75$, it follows that $u_t^r \to 0.328$, as shown in the Fig. 6b.

As previously mentioned, all the velocity profiles in the linear slip case ($\beta = 0$) for different values of b_o, intersect at a single point, $r = \left(\left(d^3+1\right)/\left(d+1\right)\right)^{1/2}$, the profile of the no-slip case ($b_o = 0$). It is easy to prove that for different values of b_o in the nonlinear slip case ($\beta \neq 0$), there is not a single point of intersection with the no-slip case, and for a given value of β and b_o, the intersection occurs at $r = \left(\left(d^3\chi_e + \chi_i\right)/\left(d\chi_e + \chi_i\right)\right)^{1/2}$, which is consistent with the previous single value of r for the linear case, $\beta = 0$ with $\chi_e = \chi_i = 1$. In Fig. 7a, b, we present detailed plots of the velocity profile for the two previous values of β considered in Fig. 2 and different values of b_o, with the circular points in the figures corresponding to the intersection points between the different slip cases and the no-slip case. The values reported in the Fig. 7a, b at the intersection points (see vertical lines) exactly coincide with the ones obtained with the above analytical estimation of the intersection points for the corresponding values of β and b_o.

Another interesting feature of the solution of the nonlinear Eq. (3.6) can be observed in the limit when $b_o \to \infty$. In this limit, $B \to 0$ as $-d^2/\left(2b_o\left(d^3+1\right)\right)$, which exactly coincides with the same limit in the linear slip case. Therefore:

$$\lim_{b_o \to \infty} (u_\theta) \to \frac{-d}{2b_o\left(d^2 + 1/d\right)}\left(\left(1-2b_o\right)r - \frac{1}{r}\right) = \frac{d^2 r}{\left(d^3+1\right)}, \quad 1 \leq r \leq d, \tag{3.12}$$

The above expression corresponds to a fluid motion in the gap between the cylinders as an attenuated dimensionless rigid body rotation, with $u_\theta = r$ as the rigid body rotation due to the motion of the inner cylinder. Consequently, in this limit the fluid behaves as a solid with a slip rotation between the solid cylinders, rotor and stator. From this result, it can be concluded that the inverted velocity profile shows the tendency of the flow field to approach the attenuated rigid body rotation limit for large values of b_o. This type of behaviour (attenuated rigid body rotation) was previously reported in [32] for the cases of

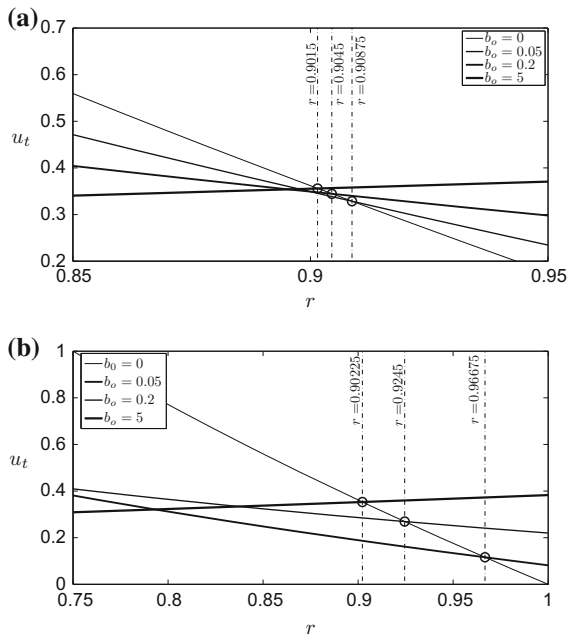

FIG. 7. Velocity profile plots for two values of β: **a** $\beta = 0.1$ and **b** $\beta = 0.5$ and their intersection with the corresponding no-slip case

linear and nonlinear Navier's slip models in the limit of large values of the slip length. This behaviour is also observed in [27] for the cases of linear slip flow described by the Navier and Langmuir's slip models, in the limit of large values of the slip length in the case of the Navier model and of a small fraction of surface covered by adsorbed atoms in the case of the Langmuir model.

4. External rotating cylinder

In the case when the external cylinder is rotating at a constant speed and the internal one is stationary, the slip boundary conditions (3.4a), (3.4b) become:

$$Ad - \frac{B}{d} = b_o \chi_i \left(\beta, \|B\|\right) \left(\frac{2B}{d^2}\right), \tag{4.1a}$$

$$A - B = 1 - b_o \chi_e \left(\beta, \|B\|\right) (2\ B), \tag{4.1b}$$

with χ_e and χ_i as previously defined. From (4.1a) and (4.1b), the following nonlinear algebraic equation for B is obtained:

$$\left[\left(1 - d^2\right) + 2b_o \left(\frac{1}{d}\chi_i \left(\beta, \|B\|\right) + d^2 \chi_e \left(\beta, \|B\|\right)\right)\right] = \frac{d^2}{B} \tag{4.2}$$

Equation (4.2) can be solved using the same two approaches described before, i.e., by a Newton iterative scheme or a graphical representation. In Fig. 8, the values of B for $d = 0.75$ and different values of b_o and β are reported. In contrast with the previous case of internal rotating cylinder, the values of B are positive instead of negative. As before, it is possible to observe the asymptotic curve $B = d^2/2\beta$ corresponding to the limit $\chi_i \to \infty$, bounding from above the possible values of B, as well as the value $B = d^2/\left(1 - d^2\right)$ corresponding to the no-slip case, i.e., the horizontal line at the top of the

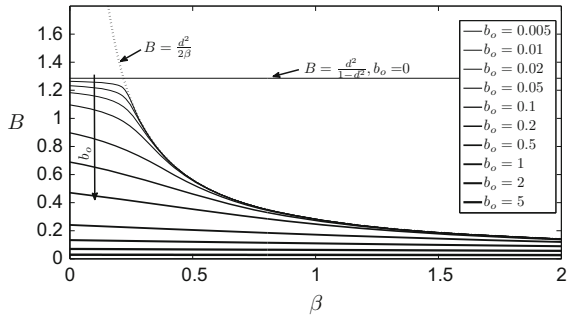

FIG. 8. Newton iterative solution of the nonlinear Eq. (4.2) for different values of β and b_o (external moving cylinder)

figure. As before, the values for the linear slip case, $B = d^2/\left(\left(1-d^2\right) + 2b_o\left(d^2 + 1/d\right)\right)$, are given by the interception of the b_o curves with the vertical axis of the figure.

After obtaining the value of B, the value of A is found from (4.1a) or (4.1b), completing the solution of the problem. By substituting the relation between the constant A and B in Eq. (3.3a), the following expression for the fluid velocity is found:

$$u_\theta = B\left[\frac{1}{d^2}\left(1 + \frac{2b_o}{d}\chi_i\right)r - \frac{1}{r}\right] \tag{4.3}$$

As in the case of the interior moving cylinder, in Fig. 8, it is possible to observe two distinct regions of possible values of B, corresponding to values of $\beta \gtrless \left(1-d^2\right)/2$ ($\beta \gtrless 0.21875$ for $d = 0.75$), defined by the point where the asymptotic curve $B = d^2/2\beta$ attains the value of the no-slip case $B = d^2/\left(1-d^2\right)$. For values of $\beta \leq \left(1-d^2\right)/2$, the value of B decreases monotonically with b_o in the range $0 \leq B \leq d^2/\left(1-d^2\right)$, which can be shown to correspond to a monotonic decreasing function of the slip velocity at the moving exterior cylinder with respect to b_o. On the other hand, for $\beta > \left(1-d^2\right)/2$ the value of B is limited to the range $0 \leq B \leq d^2/2\beta$, with a resulting non-monotonic function of the slip velocity at the moving cylinder with respect to b_o, presenting a discontinuous limit as $b_o \to 0$ given by $u_t^r \to \left(1-d^2\right)/(2\beta)$, with $u_t^r = 1$ at $b_o = 0$.

The above results are consistent with the previous results of the interior moving cylinder, and therefore will only be briefly described here. One major difference with the interior rotating cylinder case is that inverted velocity profiles are not observed when the exterior cylinder rotates. By looking at the possibility of having the velocity at the moving exterior cylinder equal to the velocity at the stationary interior one, i.e., from (4.3) when

$$\frac{1}{d^2}\left(1 + \frac{2b_o}{d}\chi_i\right) - 1 = \frac{1}{d}\left(\frac{1}{d}\left(1 + \frac{2b_o}{d}\chi_i\right) - 1\right), \tag{4.4}$$

it follows that $b_o = -d\left(1+d\right)/\left(2d\chi_i\right)$, which is unphysical since χ_i is always a positive quantity, given $b_o < 0$.

On the other hand, in the limit when $b_o \to \infty$, we have that $B \to 0$ as $d^2/\left(2b_o\left(d^2 + d^{-1}\right)\right)$ with $\chi_i \to 1$, and consequently in this limit

$$u_\theta \to \frac{d^2}{2b_o\left(d^2 + d^{-1}\right)}\left(\frac{2b_o}{d^3}r - \frac{1}{r}\right) = \frac{r}{\left(d^3+1\right)}, \tag{4.5}$$

which again corresponds to an attenuated rigid body rotation, with the fluid velocity at the moving exterior cylinder always faster than the fluid velocity at the interior stationary cylinder. In this case, this asymptotic limit is attained monotonically without the existence of any inverted velocity profiles.

5. Conclusions

In this work, a detailed study of the effect of Thompson and Troian's nonlinear slip model on the flow behaviour of a Newtonian incompressible fluid between two concentric rotating cylinders (Couette flow) is presented. By considering this type of nonlinear slip condition in the mathematical formulation of the problem, where the slip length depends on the tangential shear rate at the solid surface instead of being a constant value, it was possible to predict complex flow behaviour that has not been previously reported in the literature. In addition to this, we have shown the effect of the nonlinear slip condition on the inverted velocity profile, previously observed in the linear slip case.

By using the exact analytical form of the velocity and pressure fields, it was possible to rewrite the problem in terms of a nonlinear algebraic equation for a single unknown coefficient, B, which is difficult to solve using a closed-form analytical solution. However, a numerical scheme, such as the Newton iterative approach, or a graphical representation of the nonlinear algebraic equation can be used to find the value of B for giving a set of values of the problems parameters, completing the solution problem. In this work, both approaches were used to solve the resulting nonlinear algebraic equation, given exactly the same result. In the graphical representation approach, it is possible to simultaneously observe the value of B corresponding to all three slip conditions (no-slip, and linear and nonlinear slip) in a single figure.

In the case of a moving interior cylinder, an asymptote to the curves $Y_2(\beta, b_o, B)$ at $B = -d^2/2\beta$ was found, see Eq. (3.9b), which limits the range of possible values of B. For $\beta \leq d\left(1-d^2\right)/2$, the value of B in all cases (no-slip, linear and nonlinear slip) are found inside the range $-d/\left(1-d^2\right) \leq B \leq 0$. On the other hand, for values of $\beta > d\left(1-d^2\right)/2$, the no-slip and linear slip cases are inside the range $-d/\left(1-d^2\right) \leq B \leq 0$, while in the nonlinear case $-d^2/2\beta \leq B \leq 0$.

By looking at the analytical form of the solution, it is found that at $b_o = (1+d)/(2d\chi_e)$, with $\chi_e = (1-2\beta\|B\|)^{-1/2}$, the fluid velocity at the moving rotor is equal to the velocity at the stationary stator, while for values of $b_o > (1+d)/(2d\chi_e)$ inverted velocity profiles occur, with the fluid at the stationary stator moving faster than at the moving rotor.

In the nonlinear case, a new and non-trivial feature appears in the behaviour of the slip velocity. In all cases ($\beta \lesseqgtr d\left(1-d^2\right)/2$), the slip velocity at the stator is a monotonic increasing function of b_o, while for $\beta \leq d\left(1-d^2\right)/2$, the slip velocity at the rotor is a monotonic decreasing function of b_o; however, for $\beta > d\left(1-d^2\right)/2$, the slip velocity at the rotor is not a monotonic function having a local maximum near $b_o = 0$. Besides, when $\beta > d\left(1-d^2\right)/2$, the rotor slip velocity has a jump condition at $b_o = 0$ with a value of $u_t^r = 1$ at $b_o = 0$, according to the no-slip condition, but with a limiting value smaller than one as $b_o \to 0$, i.e., a discontinuous limit. This particular behaviour on the solution is due to the apparent singularity on the slip length in Thompson and Troian's nonlinear model, which results in a regular flow field attained only in the limit as $b_o \to 0$. In the present case, this result contradicts previous critiques of Thompson and Troian's nonlinear model corresponding to the behaviour of the flow field near the critical shear rate (apparent singular slip length), since in such a limit, the flow field tends to a slip flow with finite slip length.

For the linear slip case, it is known that all velocity profiles for different values of b_o intersect at a single point, $r = \left(\left(d^3+1\right)/(d+1)\right)^{1/2}$, the profile of the no-slip case. However, in the nonlinear slip case, it was found that there is not a single point of intersection and for given values of β and b_o, the intersection occurs at $r = \left(\left(d^3\chi_e + \chi_i\right)/(d\chi_e + \chi_i)\right)^{1/2}$.

Another interesting feature of the solution of the obtained nonlinear algebraic equation is found in the limit when $b_o \to \infty$, for a given finite value of β. In this limit, $B \to 0$ as $-d^2/\left(2b_o\left(d^3+1\right)\right)$ with the fluid velocity tending to an attenuated rigid body rotation. Therefore, in this limit, the fluid in the gap behaves as a rotating solid ring slipping between the two solid cylinders. From this result, it can be concluded that the so-called inverted velocity profile shows the tendency of the flow field to approach the

attenuated rigid body rotation limit, with faster velocity at the outer boundary than any other internal point.

Similar results to those mentioned above for the internal rotating cylinder are found in the case of a rotating external cylinder, including the attenuated rigid body rotation limit for large value of b_o. However, in this case it is not possible to observe inverted velocity profiles, which is a consequence of the asymptotic attenuated rigid body rotation limit with the fluid velocity in contact with the external rotating cylinder moving faster than at any other point.

Acknowledgements

Part of the work reported here is included in the research projects of Mr. J. Soavi and Mr. P. Kantachuvesiri required for their undergraduate degree.

References

1. Barber, R.W., Sun, Y., Gu, X.J., Emerson, D.R.: Isothermal slip flow over curved surfaces. Vacuum **76**, 73–81 (2004)
2. Neto, C., Evans, D., Bonaccurso, E., Butt, H., Craig, V.: Boundary slip in Newtonian liquids: a review of experimental studies. Rep. Prog. Phys. **68**(12):2859–2897, (2005)
3. Willmott, G.R., Tallon, J.L.: Measurement of Newtonian fluid slip using a torsional ultrasonic oscillator. Phys. Rev. E. **76**, 066306-1–066306-12 (2007)
4. Zhu, Y., Granick, S.: Rate-dependent slip of Newtonian liquid at smooth surfaces. Phys. Rev. Lett. **87**, 096105–096105-4 (2001)
5. Thompson, P.A., Troian, S.M.: A general boundary condition for liquid flow at solid surfaces. Nature **389**, 360–362 (1997)
6. Priezjev, N.V.: Molecular dynamics simulations of oscillatory Couette flows with slip boundary conditions. Microfluid Nanofluid **14**, 225–233 (2013)
7. Navier, C.L.M.H.: Memoire sur les lois du mouvement des fluids. Mem. Acad. Sci. Inst. Fr. **6**, 389–416 (1829)
8. Maxwell, J.C.: On stresses in rarified gases arising from inequalities in temperature. Philos. Trans. R. Soc. Part. **1170**, 231–256 (1879)
9. Nieto, C., Giraldo, M., Power, H.: Boundary integral equation approach for Stokes slip flow in rotating mixers. Discret. Contin. Dyn. Syst. Ser. B **15**(4), 1019–1044 (2011)
10. Gad-el-Hak, M.: MEMS: Introduction and Fundamentals. Taylor and Francis, Boca Raton (2006)
11. Xiaojin, W., Joshi, Y.: Experimental and numerical study of sidewall profile effects on flow and heat transfer inside microchannels. Int. J. Heat Mass Transfer **50**, 4640–4651 (2007)
12. Lilley, C.R., Sader, J.E.: Velocity profile in the Knudsen layer according to the Boltzmann equation. Proc. R. Soc. London, Ser. A **464**, 2015–2035 (2008)
13. Bowles, A.P., Ducker, W.A.: Gas flow near a smooth plate. Phys. Rev. E. **83**, 056328–056332 (2011)
14. Seo, D., Ducker, W.A.: In situ control of gas flow by modification of gas–solid interactions. Phys. Rev. Lett. **111**, 174502–174506 (2013)
15. Choi, C.H., Kim, C.J.: Large slip of aqueous liquid flow over a nanoengineered superhydrophobic surface. Phys. Rev. Lett. **96**(6), 066001–066005 (2006)
16. Yang, F.: Slip boundary condition for viscous flow over solid surfaces. Chem. Eng. Commun. **197**, 544–550 (2010)
17. Pit, R., Hervet, H., Leger, L.: Friction and slip of a simple liquid at a solid surface. Tribol. Lett. **7**, 147–152 (1999)
18. Hoa, T.A., Papavassilioua, D.V., Leeb, L.L., Strioloa, A.: Liquid water can slip on a hydrophilic surface. Proc. Natl. Acad. Sci. USA, **108**(39), 16170–16175, (2011)
19. Bonaccurso, E., Kappl, M., Butt, Hans-Jrgen: Hydrodynamic force measurements: boundary slip of water on hydrophilic surfaces and electrokinetic effects. Phys. Rev. Lett. **88**(7), 0761031–0761034 (2002)
20. Priezjev, N.V., Troian, S.M.: Molecular origin and dynamic behavior of slip in sheared polymer films. Phys. Rev. Lett. **92**, 018302-1–018302-4 (2004)
21. Zhou, P., Cheng-wei, W., Guo-jun, M.: Nonlinear boundary slip of fluid flowing over solid surface. J. Cent. South Univ. Technol. **14**, 30–33 (2007)
22. Atwood, B.T., Schowalter, W.R.: Measurements of slip at the wall during flow of high-density polyethylene through a rectangular conduit. Rheol. Acta **28**, 134–146 (1989)

23. Darbandi, M., Mahboubi Fouladi, H., Zakyani, M., Schneider, G.E.: Numerical simulation of slip flow through microchannels; described in the curvilinear coordinate system. In: Proceedings of the International Conference on Mechanical Engineering and MechatronicsToronto, (2013), Ontario, Canada
24. Matthews, M.T., Hill, J.M.: Newtonian flow with nonlinear Navier boundary condition. Acta Mech. **191**, 195–217 (2007)
25. Spikes, H., Granick, S.: Equation for slip of simple liquids at smooth solid surfaces. Langmuir **19**, 5065–5071 (2003)
26. Yuhong, S., Barber, R.W., Emerson, D.R.: Inverted velocity profiles in rarefied cylindrical Couette gas flow and the impact of the accommodation coefficient. Phys. Fluids **17**, 047102–10471027 (2005)
27. Myong, R.S., Reese, J.M., Barber, R.W., Emerson, D.R.: Velocity slip in microscale cylindrical Couette flow: the Langmuir model. Phys. Fluids **17**, 087105-1–087105-11 (2005)
28. Eijkel, J.: Liquid slip in micro- and nanofluidics: recent research and its possible implications. Lab Chip **7**, 299–301 (2007)
29. Nguyen, N., Wereley, S.: Fundamentals and Applications of Microfluidics. Artech House, Norwood (2006)
30. Karniadakis, G., Beskok, A., Gad-el-Hak, M.: Microflows and nanoflows: fundamentals and simulation. Appl. Mech. Rev. **55**(4), 1–76 (2002)
31. Sajid, M., Awais, M., Nadeem, S., Hayat, T.: The influence of slip condition on thin film flow of a fourth grade fluid by the homotopy analysis method. Comput. Math. Appl. **56**, 2019–2026 (2008)
32. Nieto, C., Giraldo, M., Power, H.: Boundary elements solution of Stokes flow between curved surfaces with nonlinear slip boundary condition. Numer. Methods Partial Differ. Equ. **29**(3), 757–777 (2012)

H. Power
Division of Energy and Sustainability
University of Nottingham
University Park
Nottingham
NG7 2RD
UK
e-mail: henry.power@nottingham.ac.uk

J. Soavi
Department of Hydraulic and Fluid Mechanics
ENSEEIHT
Toulouse
France

P. Kantachuvesiri
Division of Energy and Sustainability
University of Nottingham
University Park
Nottingham
NG7 2RD
UK

C. Nieto
Grupo de Energia y Termodinmica Facultad de Ingeniera Aeronutica
Circular 1 No. 7-01
Universidad Pontificia Bolivariana
Sede Central Medellín
Medellín
Colombia
e-mail: cesar.nieto@upb.edu.co

(Received: July 15, 2014; revised: April 1, 2015)